NASA CR-111962

COMPUTING DISPERSAL OF ATMOSPHERIC POLLUTANTS NEAR AIRPORTS

Coleman duP. Donaldson and Glenn R. Hilst

Prepared under Contract NAS1-10192 by
Aeronautical Research Associates of Princeton, Inc.
50 Washington Road, Princeton, New Jersey 08540

for

NATIONAL AERONAUTICS AND SPACE ADMINISTRATION

July 1971

NASA CR-111962

A.R.A.P. Report 162

COMPUTING DISPERSAL OF ATMOSPHERIC POLLUTANTS NEAR AIRPORTS

Coleman duP. Donaldson and Glenn R. Hilst

Prepared under Contract NAS1-10192 by

Aeronautical Research Associates of Princeton, Inc.
50 Washington Road, Princeton, New Jersey 08540

for

NATIONAL AERONAUTICS AND SPACE ADMINISTRATION

July 1971

ERRATA

NASA CR-111962

Page 32, Figure 6A — scales for $\overline{C_p'T'}$ and $\overline{C_p'w'}$ should be offset to the right to coincide with the position shown in figure 5A

COMPUTING DISPERSAL OF ATMOSPHERIC POLLUTANTS NEAR AIRPORTS

Coleman duP. Donaldson and Glenn R. Hilst
Aeronautical Research Associates of Princeton, Inc.

SUMMARY

This report summarizes the results of the first year of effort under Contract NAS1-10192 between NASA and A.R.A.P. The objective of this Phase I effort has been the application of the methods of invariant modeling of turbulent shear flows and atmospheric dispersion of conservative pollutants to the problem of air pollution in the vicinity of airports. Although aircraft operations in general do not constitute a major contribution to the nation's air quality problems, the contributions of exhaust products in taxi, idle, take-off, and landing modes at airports do pose a potential major local air pollution problem in the vicinity of airports. The detailed understanding of the genesis and extent of this problem, with appropriate recognition of the unusual features of aircraft operation near and on the ground (e.g., accelerations of moving sources, aircraft-induced vortical motions, etc.), justifies the very detailed insights which invariant modeling provides.

The results of this work to date show that, with only minimum information input (mean wind and temperature profiles), the invariant modeling technique predicts the structure of atmospheric turbulence and associated fluxes of atmospheric properties, such as heat, momentum, and gaseous pollutant matter, within very useful limits of accuracy. It is also evident that these accuracies can be improved by further comparison of predicted and experimental measurements of these quantities, using a thorough parameter search for the model's specification of the scale lengths which control the generation and dissipation of turbulent correlations. The demonstrated successes to date more than justify the further development and application of these techniques to specialized and complicated problems, such as local airport pollution phenomena.

The production of a working model of atmospheric dispersion appropriate to line sources has been achieved. A comparable model for point sources has been programmed but has not been finally debugged. Time and resources have permitted only preliminary application of this model to the airport problem. These results do, however, demonstrate the feasibility of application of the model to complex aircraft operation modes in the vicinity of airports.

INTRODUCTION

In cataloging the causes of environmental quality changes and the role of federal activities in promoting land usages which enhance these causes, the President's Council on Environmental Quality has noted the following facts with regard to airports: "...But airports also have significant environmental impact. They bring high noise level, new access highways, air pollution from automobiles and aircraft, and sewage and solid waste disposal problems." (ref. 1) Among these problems, the work reported here is directed to providing the advanced technology necessary to evaluate the nature and magnitude of the air pollution problem in the vicinity of airports and to evaluate the effectiveness and costs of alternative methods for either controlling the air quality levels or protecting those who are exposed to these hazards.

With this rationale in mind, the National Aeronautics and Space Administration (NASA) and Aeronautical Research Associates of Princeton, Inc. (A.R.A.P.) entered into Contract NAS1-10192 in July 1970, as Phase 1 of a continuing research and development effort. The objectives for Phase 1 were:

> "The development of a program for and the calculation of the meteorological parameters and distribution of pollutants in the vicinity of an airport for any given upstream meteorological conditions when the absorption of solar radiation by pollutants is not large." (ref. 2)

In particular, it was agreed that the methods of invariant modeling developed by Coleman duP. Donaldson, the Principal Investigator, would be developed to show their appropriateness to the problem of predicting the structure of atmospheric turbulence in the vicinity of the ground and, with this demonstration, a model capable of predicting the dispersal of inert airborne pollutants emanating from arbitrary source configurations would be constructed and tested.

These objectives have been achieved and the results are reported here. In completing Phase 1, the understanding and insights necessary for further refinement and application of these models to airport problems have also been advanced. The avenues of most productive continuation of this work have been submitted to NASA as a continuation proposal for this work (ref. 3).

This report is divided into two major sections. The first presents the basic rationale of invariant modeling and the demonstration and verification of the validity of this modeling technique in specifying the structure of atmospheric turbulence near the ground. The second section presents the basic model for atmospheric dispersion of materials emanating from arbitrarily positioned line and point sources. This model depends upon the turbulence model for inputs of turbulence structure and, when the

source configuration is specified, predicts the distribution of pollutant concentration downstream. Only simple source configurations have been used to demonstrate the model's validity. The extension to moving and accelerating sources, as well as to multiple sources, is a straightforward extension of this work.

SYMBOLS

a, b, c	"universal" constants, equations 11 and 14
$\overline{C}_N$	normalized mass fraction of pollutant
C_P	pollutant concentration (mass fraction)
g	acceleration of gravity
K	$\overline{u'^2} + \overline{v'^2} + \overline{w'^2}$ (turbulent kinetic energy)
$\dot{m}_p$	source strength of pollutant
Re_Λ	turbulence Reynolds numbers
$\overline{T}, T'$	temporal mean and local fluctuations of temperature
t	time
$\bar{u}, \bar{v}, \bar{w}$	time-averaged components of fluid motion
u', v', w'	turbulent components of fluid motion
V_{eff}	velocity of source relative to air
x, y, z	cartesian coordinate system chosen so that $\overline{v'}=\overline{w'}\equiv 0$
X	body force
Λ, λ	diffusivity and dissipation coefficients associated with invariant modeling of turbulent fluid flows
τ	time of exposure
μ_o	diffusivity
μ_2	second viscosity coefficient
ρ_o	density of mixture of gases
δ_{eff}	effective boundary layer thickness

COMPUTATIONS OF THE GENERATION OF TURBULENCE IN THE ATMOSPHERIC BOUNDARY LAYER

In several previous papers (refs. 4, 5, and 6), we have discussed in some detail the theoretical basis for a new method of calculating the development of turbulent shear layers. The essence of this method is a closure of the equations of turbulent motion that are derived from the Navier-Stokes equations by a modeling of the unknown terms in the equations for the second-order correlations of fluctuating quantities. We have applied the equations obtained in this way to the generation of turbulence in a free shear layer in the atmosphere (ref. 5). More recently, we have applied the method to the calculation of the turbulent kinetic energy and the transport of heat and momentum in the earth's boundary layer. For this case of the generation of atmospheric turbulence, the results of computations can be compared with detailed experimental results made available to us by John Wyngaard and Owen Coté of the U.S. Air Force Cambridge Research Laboratories. The agreement between calculated and experimental results has been most gratifying. The role played by the scale of atmospheric turbulence in determining the intensity of turbulence generated by a given shear layer can be investigated by means of these calculations, and the results we have obtained have been most instructive.

Basic Equations

The basic equations for the generation of turbulence in a parallel shearing motion in the atmosphere obtained by the method of invariant modeling (ref. 5), and under the assumptions μ_o = constant, Schmidt number = Prandtl number = 1.0, are

$$\rho_o \frac{\partial \bar{u}}{\partial t} = \mu_o \frac{\partial^2 \bar{u}}{\partial z^2} - \frac{\partial}{\partial z}\left(\rho_o \overline{u'w'}\right) + X(z,t) \tag{1}$$

$$\rho_o \frac{\partial \bar{T}}{\partial t} = \mu_o \frac{\partial^2 \bar{T}}{\partial z^2} - \frac{\partial}{\partial z}\left(\rho_o \overline{T'w'}\right) + Q(z,t) \tag{2}$$

$$\frac{\partial \overline{u'u'}}{\partial t} = -2\overline{u'w'}\frac{\partial \bar{u}}{\partial z} + \frac{1}{\rho_o}\frac{\partial}{\partial z}\left(\rho_o \sqrt{K}\Lambda \frac{\partial \overline{u'u'}}{\partial z}\right) - \frac{\sqrt{K}}{\Lambda}\left(\overline{u'u'} - \frac{K}{3}\right) + \frac{\mu_o}{\rho_o}\frac{\partial^2}{\partial z^2}\overline{u'u'} - \frac{2\mu_o}{\rho_o}\frac{\overline{u'u'}}{\lambda^2} \tag{3}$$

$$\frac{\partial \overline{v'v'}}{\partial t} = \frac{1}{\rho_o}\frac{\partial}{\partial z}\left(\rho_o\sqrt{K}\Lambda\frac{\partial \overline{v'v'}}{\partial z}\right) - \frac{\sqrt{K}}{\Lambda}\left(\overline{v'v'} - \frac{K}{3}\right)$$

$$+ \frac{\mu_o}{\rho_o}\frac{\partial^2}{\partial z^2}\overline{v'v'} - \frac{2\mu_o}{\rho_o}\frac{\overline{v'v'}}{\lambda^2} \qquad (4)$$

$$\frac{\partial \overline{w'w'}}{\partial t} = \frac{1}{\rho_o}\frac{\partial}{\partial z}\left(3\rho_o\sqrt{K}\Lambda\frac{\partial \overline{w'w'}}{\partial z}\right) - \frac{\sqrt{K}}{\Lambda}\left(\overline{w'w'} - \frac{K}{3}\right)$$

$$+ \frac{2}{\rho_o}\frac{\partial \rho_o}{\partial z}\left(\Lambda\sqrt{K}\frac{\partial \overline{w'w'}}{\partial z}\right) + \frac{2}{\rho_o}\frac{\partial}{\partial z}\left(\rho_o\sqrt{K}\Lambda\frac{\partial}{\partial z}\overline{w'w'}\right)$$

$$+ \frac{\mu_o}{\rho_o}\frac{\partial^2}{\partial z^2}\overline{w'w'} - \frac{2\mu_o}{\rho_o}\frac{\overline{w'w'}}{\lambda^2}$$

$$- \frac{2(\mu_o+\mu_2)}{\rho_o}\left\{\overline{w'w'}\left[\frac{\partial}{\partial z}\left(\frac{1}{\rho_o}\frac{\partial \rho_o}{\partial z}\right) - \frac{1}{\rho_o^2}\left(\frac{\partial \rho_o}{\partial z}\right)^2\right]\right\}$$

$$+ \frac{2g}{T_o}\overline{w'T'} \qquad (5)$$

$$\frac{\partial \overline{u'w'}}{\partial t} = -\overline{w'w'}\frac{\partial \bar{u}}{\partial z} + \frac{2}{\rho_o}\frac{\partial}{\partial z}\left(\rho_o\sqrt{K}\Lambda\frac{\partial}{\partial z}\overline{u'w'}\right)$$

$$+ \frac{1}{\rho_o}\frac{\partial}{\partial z}\left(\rho_o\sqrt{K}\Lambda\frac{\partial}{\partial z}\overline{u'w'}\right) - \frac{\sqrt{K}}{\Lambda}\overline{u'w'} + \frac{\Lambda\sqrt{K}}{\rho_o}\frac{\partial}{\partial z}\overline{u'w'}\frac{\partial \rho_o}{\partial z}$$

$$+ \frac{\mu_o}{\rho_o}\frac{\partial^2}{\partial z^2}\overline{u'w'} - \frac{2\mu_o}{\rho_o}\frac{\overline{u'w'}}{\lambda^2}$$

$$- \frac{(\mu_o+\mu_2)}{\rho_o}\left\{\overline{u'w'}\frac{\partial}{\partial z}\left(\frac{1}{\rho_o}\frac{\partial \rho_o}{\partial z}\right) - \frac{\overline{u'w'}}{\rho_o^2}\left(\frac{\partial \rho_o}{\partial z}\right)^2\right\}$$

$$+ \frac{g}{T_o}\overline{u'T'} \qquad (6)$$

$$\frac{\partial \overline{u'T'}}{\partial t} = -\overline{u'w'}\,\frac{\partial \bar{T}}{\partial z} - \overline{w'T'}\,\frac{\partial \bar{u}}{\partial z} + \frac{1}{\rho_o}\frac{\partial}{\partial z}\left(\rho_o\sqrt{K}\Lambda\frac{\partial \overline{u'T'}}{\partial z}\right)$$

$$- \frac{\sqrt{K}}{\Lambda}\overline{u'T'} + \frac{\mu_o}{\rho_o}\frac{\partial^2}{\partial z^2}\overline{u'T'} - \frac{2\mu_o}{\rho_o}\frac{\overline{u'T'}}{\lambda^2} \qquad (7)$$

$$\frac{\partial \overline{w'T'}}{\partial t} = -\overline{w'w'}\,\frac{\partial \bar{T}}{\partial z} + \frac{2}{\rho_o}\frac{\partial}{\partial z}\left(\rho_o\sqrt{K}\Lambda\frac{\partial \overline{w'T'}}{\partial z}\right)$$

$$+ \frac{1}{\rho_o}\frac{\partial}{\partial z}\left(\rho_o\sqrt{K}\Lambda\frac{\partial}{\partial z}\overline{w'T'}\right) - \frac{\sqrt{K}}{\Lambda}\overline{w'T'}$$

$$+ \frac{\mu_o}{\rho_o}\frac{\partial^2}{\partial z^2}\overline{w'T'} - \frac{2\mu_o}{\rho_o}\frac{\overline{w'T'}}{\lambda^2}$$

$$- \frac{(\mu_o+\mu_2)}{\rho_o}\left\{\overline{T'w'}\,\frac{\partial}{\partial z}\left(\frac{1}{\rho_o}\frac{\partial \rho_o}{\partial z}\right) - \frac{\overline{w'T'}}{\rho_o^2}\left(\frac{\partial \rho_o}{\partial z}\right)^2\right\}$$

$$+ \frac{g}{T_o}\overline{T'^2} \qquad (8)$$

$$\frac{\partial \overline{T'^2}}{\partial t} = -2\overline{w'T'}\,\frac{\partial \bar{T}}{\partial z} + \frac{1}{\rho_o}\frac{\partial}{\partial z}\left(\rho_o\sqrt{K}\Lambda\frac{\partial}{\partial z}\overline{T'^2}\right)$$

$$+ \frac{\mu_o}{\rho_o}\frac{\partial^2}{\partial z^2}\overline{T'^2} - \frac{2\mu_o}{\rho_o}\frac{\overline{T'^2}}{\lambda^2} \qquad (9)$$

$$K = \overline{u'^2} + \overline{v'^2} + \overline{w'^2} \qquad (10)$$

$$\lambda = \Lambda/\sqrt{a + b \cdot Re_\Lambda} \qquad (11)$$

$$Re_\Lambda = \rho\sqrt{K}\Lambda/\mu_o \qquad (12)$$

$$\Lambda = c\delta_{eff} \qquad z > c\delta_{eff}/\sqrt{a} \qquad (13)$$

$$\Lambda = \sqrt{a}\,z \qquad 0 \le z \le c\delta_{eff}/\sqrt{a} \qquad (14)$$

The term $q(z,t)$ in Eq. (2) can be used to represent a local heat production or absorption layer within the atmosphere, while the term $X(z,t)$ in Eq. (1) is a forcing function that can be used to generate any desired shear layer in order to study the formation and decay of turbulence in such a layer.

In the studies we will report here, we will choose the values of the three constants a, b, and c in Eqs. (11) and (13) to be the same as used in our previous work (ref. 5), namely, $a = 2.5$, $b = 0.125$, and $c = 0.064$.

Results of Computations

Equations (1) through (14) provide a closed set for the prediction of the mean profiles of wind and temperature, $\bar{u}(z)$ and $\bar{T}(z)$, the intensity of turbulence, $\overline{u'^2}$, $\overline{v'^2}$, and $\overline{w'^2}$, and the fluxes of momentum and of sensible heat due to both molecular and eddy transfers. In the most general use of the model, it is necessary to specify the initial conditions on all these terms and the boundary conditions at the surface. For example, we may specify the atmosphere initially at rest, no internal sources of heat, an insulated surface (no heat transfer), and a body force which is some specified function of time (in our calculations, this serves the same purpose as a pressure gradient).

The boundary condition on the flux of momentum and heat is specified by the fact that all components of motion other than those associated with molecular diffusion must vanish at the solid boundary. The model retains these molecular transfer terms for precisely this reason, and it develops a laminar sublayer in which the molecular transfer terms are dominant and of such a magnitude as to balance the turbulent flux of heat and momentum in the atmosphere immediately above the laminar sublayer. (Consideration of the transfer rates for heat in the soil or water has not been incorporated as yet. Rather, for this early stage, the solid surface has been implicitly assumed to have an infinite heat capacity.)

Although in principle it is unnecessary to assume any upper boundary conditions in the turbulent atmosphere, other than that the vertical gradients of velocity and temperature vanish somewhere, in practise it is desirable to limit the depth of fluid considered so as to avoid excessive computer capacity requirements. In these early uses of the model, the depth of atmosphere considered has been limited by assuming that the gradients of wind and temperature go to zero at a finite height which is large compared with the depth of the atmosphere under modeling consideration. Above this

height, the model predicts no local generation of turbulence or turbulent fluxes, but it does retain the molecular flux terms. Under this assumption, the upper atmosphere is also a sink for heat and momentum. The relaxation of this practical constraint following these initial tests of the model poses no problem other than larger computer capacity and speed.

Because our initial interests during this early stage of modeling were largely directed to simulation of boundary layer turbulent fluxes of matter, the method of solution of equations (1) through (14) was modified by decoupling equations (1) and (2) and using given mean wind and temperature profiles to derive the system of equations, rather than body forces and heat sources. The equations were then used to predict the second-order correlations $\overline{u_i' u_k'}(z)$, $\overline{u_i' T'}(z)$, and $T'^2(z)$ that develop at large times when equations (3) through (9) are solved subject to any initial distribution of small turbulent velocity fluctuations. In effect, this method of solution specifies fixed mean profiles of wind and temperature and requires the model to generate those components of turbulent and molecular fluxes which these profiles would sustain in a steady-state condition.

Since the model predicts fluxes of heat and momentum to the boundary, heat sources and momentum sources must be included to maintain a steady state. The method of solution described in the previous paragraph provides these sources by restoring any deficit at each height and with each calculation step. These pseudo-sources must be of the same magnitude as the pressure gradient and heat flux terms which they balance. Of more concern is the possibility that the accelerations they represent are large and significant in the generation of turbulent fluxes. This possibility may be checked by calculating the ratio of the eddy stress $\overline{u'w'}$ to either the balancing pressure gradient force $\partial p/\partial y$ or to the coriolis acceleration $2\Omega\bar{u} \sin \phi$, where p is pressure, Ω is the rotation rate of the earth, and ϕ is the latitude. These calculations show that this ratio is order of 10^{-2}, i.e., the implied restorative body force is much smaller than the flux which it is modifying and the computation is quite stable.

The computations we shall report here were carried out for three measured mean velocity and temperature profiles supplied to us by Messrs. Wyngaard and Coté. The mean profiles were determined to a height of 32 meters by tower measurements. Beyond this height, we have had to extrapolate the velocity and temperature profiles by the often used but somewhat disturbing technique of "eyeball" continuation.

The mean profiles of velocity and temperature that were determined in this way are shown in figures 1, 2, and 3. In each

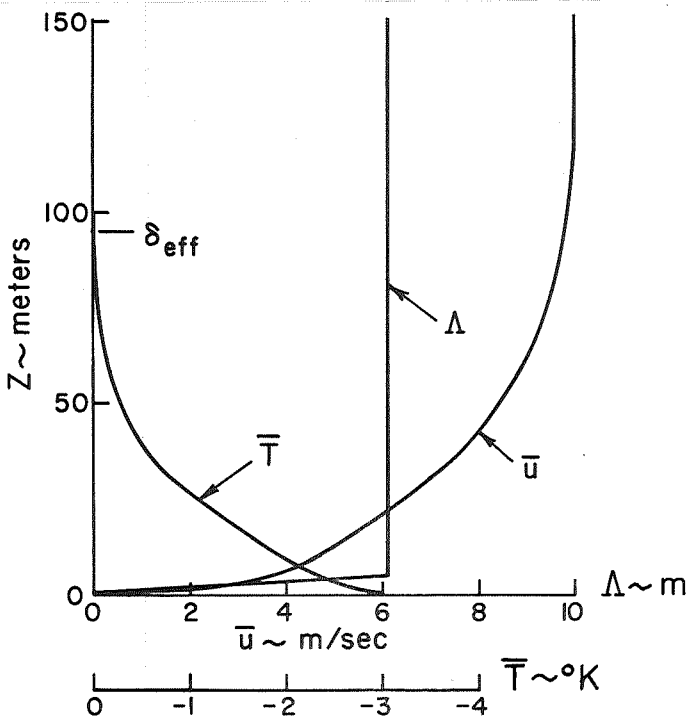

Figure 1.- Stable velocity profile - measured (to 32 m) distributions of $\bar{u}$ and $\bar{T}$ and distribution of Λ used in calculation.

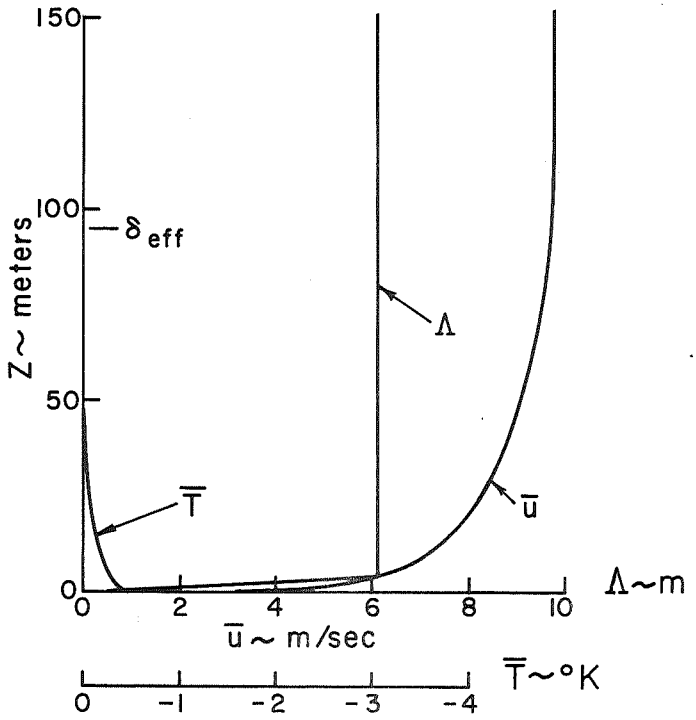

Figure 2.- Approximately neutral profile - measured (to 32 m) and extended distributions of $\bar{u}$ and $\bar{T}$ and distribution of Λ used in calculation.

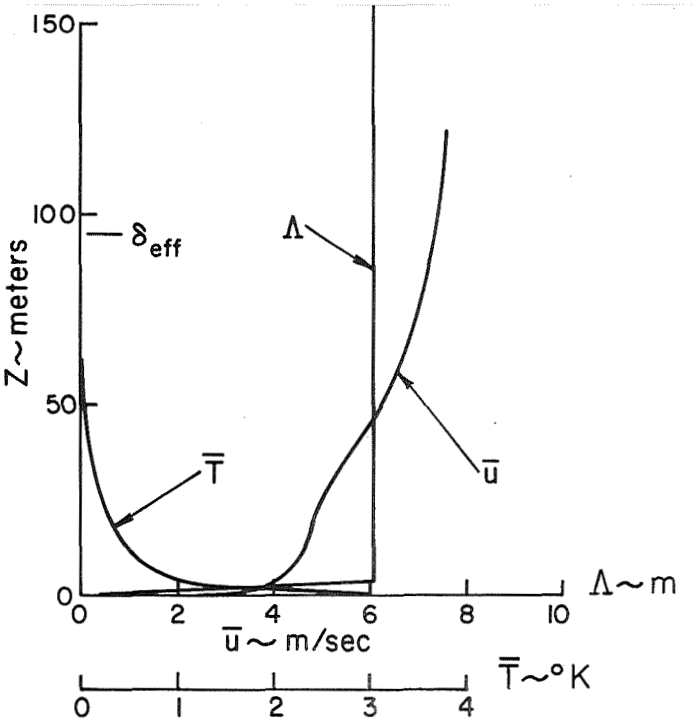

Figure 3.- Unstable profile - measured (to 32 m) and extended distributions of $\bar{u}$ and $\bar{T}$ and distribution of Λ used in calculation.

figure, we indicate the effective boundary layer height δ_{eff} that was used in the set of calculations that will be reported here, together with a plot of the scale length Λ that results from this choice of δ_{eff}.

In figures 4 through 8 we present the results of calculations of the various second-order correlations $\overline{u'u'}$, $\overline{v'v'}$, $\overline{w'w'}$, $\overline{u'w'}$, $\overline{u'T'}$, $\overline{w'T'}$, and $\overline{T'^2}$ for each of the atmospheric conditions given in figures 1 through 3. On these figures we also show the experimental measurements supplied by Wyngaard and Coté.

Examination of figures 4 and 5 shows that for a stable atmospheric situation, the model we have chosen shows rather good agreement between the calculated and measured values of both the second-order correlations $\overline{u'u'}$, $\overline{v'v'}$, $\overline{w'w'}$, and $\overline{T'^2}$ and the transport correlations $\overline{u'w'}$, $\overline{u'T'}$, and $\overline{w'T'}$. Note that the method appears to overpredict the $\overline{T'^2}$ correlation by a factor of

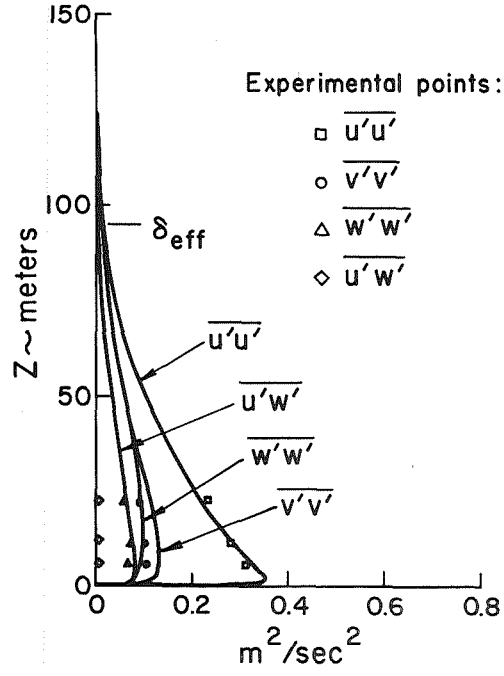

Figure 4.- Stable profile - agreement between computed and measured velocity-temperature correlation profiles.

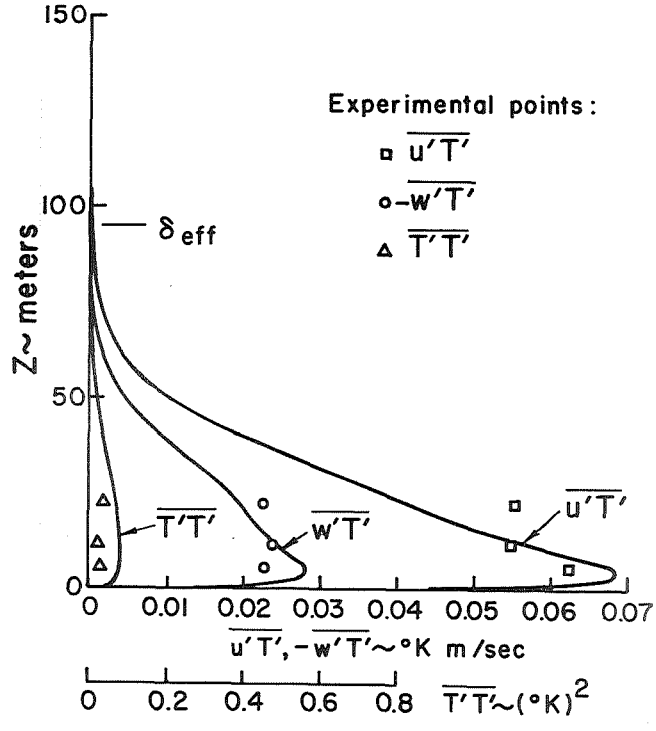

Figure 5.- Stable profile - agreement between computed and measured velocity profiles.

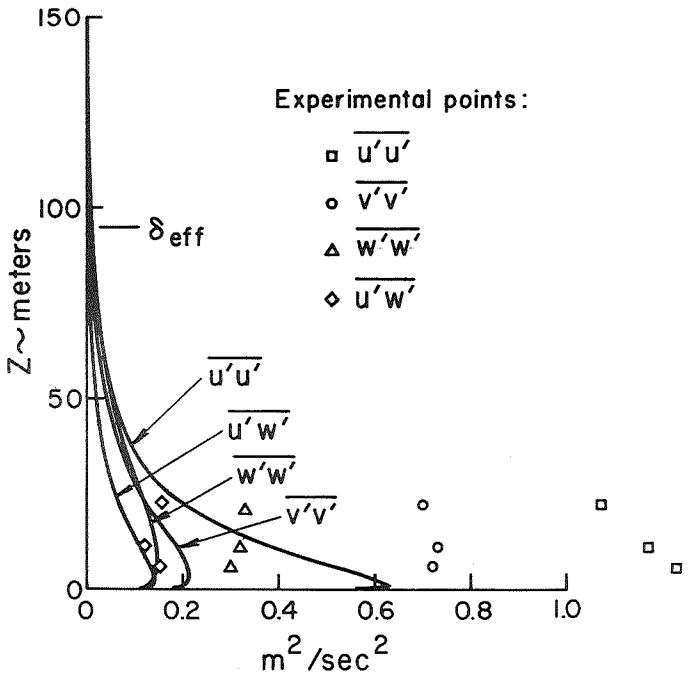

Figure 6.- Neutral profile - agreement between computed and measured velocity-temperature correlation profiles.

approximately two. The excellent agreement between measured and computed results is perhaps somewhat fortuitous because of our choice of δ_{eff} in this case, as will be discussed later.

Examination of figure 6, where we have plotted the calculated values of $\overline{u'u'}$, $\overline{v'v'}$, $\overline{w'w'}$, and $\overline{u'w'}$ and compared them with experimental measurements, shows that for this case of approximately neutral stability we generally underestimate the correlations by a factor of approximately two, although the computed level of the transport correlation $\overline{u'w'}$ is somewhat better than the others. The general character of the distributions is correct, and the authors believe that a somewhat different fairing of the mean velocity profile, so that a larger value of δ_{eff} was used in the calculation, would have resulted in there being very satisfactory agreement between theoretical and experimental results.

Examination of figures 7 and 8, where we have plotted results for an unstable atmospheric situation, indicates, for this case and with our choice of δ_{eff}, rather poor agreement between the measured values of $\overline{u'u'}$, $\overline{v'v'}$, $\overline{w'w'}$, and $\overline{T'^2}$ and the results of our calculations. It is interesting to note that the transport correlations $\overline{u'w'}$, $\overline{u'T'}$, and $\overline{w'T'}$ are predicted properly. Our

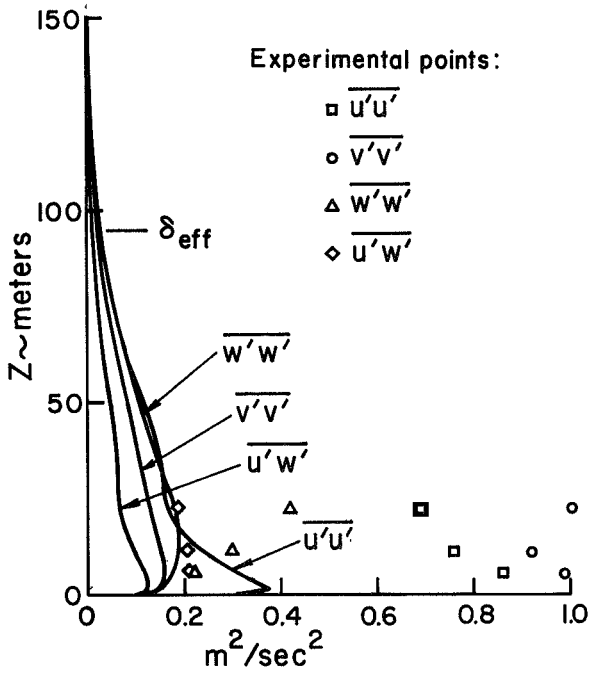

Figure 7.- Unstable profile - agreement between computed and measured velocity profiles.

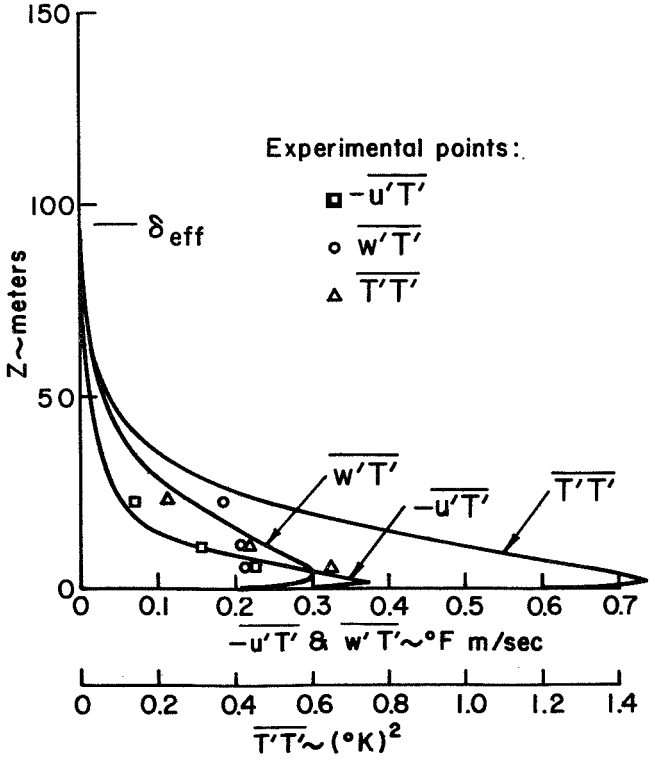

Figure 8.- Unstable profile - agreement between computed and measured velocity-temperature correlation profiles.

calculations of $\overline{u'u'}$ and $\overline{w'w'}$ are low by a factor of a little more than two, while the error in estimating $\overline{v'v'}$ is very large. At the present time we are inclined to wonder if, in this case, the very high level of $\overline{v'v'}$ that has been reported really could have been produced by the mean boundary layer profile measured below 32 meters. Perhaps the high level of $\overline{v'v'}$ could have been produced by a higher shear layer skewed in a direction so that $\bar{v}$ was important. As in the case of the neutral atmosphere, we also find for the unstable calculation that better agreement between theory and experiment for the correlation $\overline{u'u'}$ and $\overline{w'w'}$ could have been achieved by choosing a larger value for δ_{eff} . In this case, slightly poorer agreement between calculated and measured values of the transport correlations $\overline{u'w'}$, $\overline{u'T'}$, and $\overline{w'T'}$ and the temperature fluctuation $\overline{T'^2}$ would have resulted.

Since in all cases, the choice of δ_{eff} plays an important role, and it is obvious from a perusal of figures 1, 2, and 3 that the choice of δ_{eff} is quite arbitrary, it is important to investigate the sensitivity of our results to this choice. Since the choice of δ_{eff} affects the turbulence scale Λ that is used in our computations, we will, in effect, study the effect of turbulence scale on the generation of turbulence in a given shear layer by making computations for a fixed pair of mean profiles $\bar{u}(z)$ and $\bar{T}(z)$ and choosing different values of δ_{eff} when making these computations.

In figure 9, we present, for the neutral profile shown in figure 1, the results of a number of computations using different values of δ_{eff} or Λ_{max} . We have plotted in this figure the maximum values of $\overline{u'w'}$, $\overline{T'^2}$, and $K = \overline{u'^2} + \overline{v'^2} + \overline{w'^2}$ obtained in each computation as a function of δ_{eff} and Λ_{max} .

Several interesting points are immediately obvious from a study of figure 9. First we see that, for a given mean shear layer, there is a value of δ_{eff} or Λ_{max} that yields a maximum in the turbulent energy that is generated by the shear layer. The physics of this behavior of the solutions is as follows. If the scale Λ is very small, the amount of turbulent energy that can be developed by the shear layer is small because viscous dissipation rapidly kills off the energy that is produced. On the other hand, if the scale of turbulence is very large, the local turbulence level is low in the region of shear production because the energy produced by the shear is diffused rapidly to regions where the mean shear is low and the small rate of production can be balanced by the low rate of dissipation possible with large Λ .

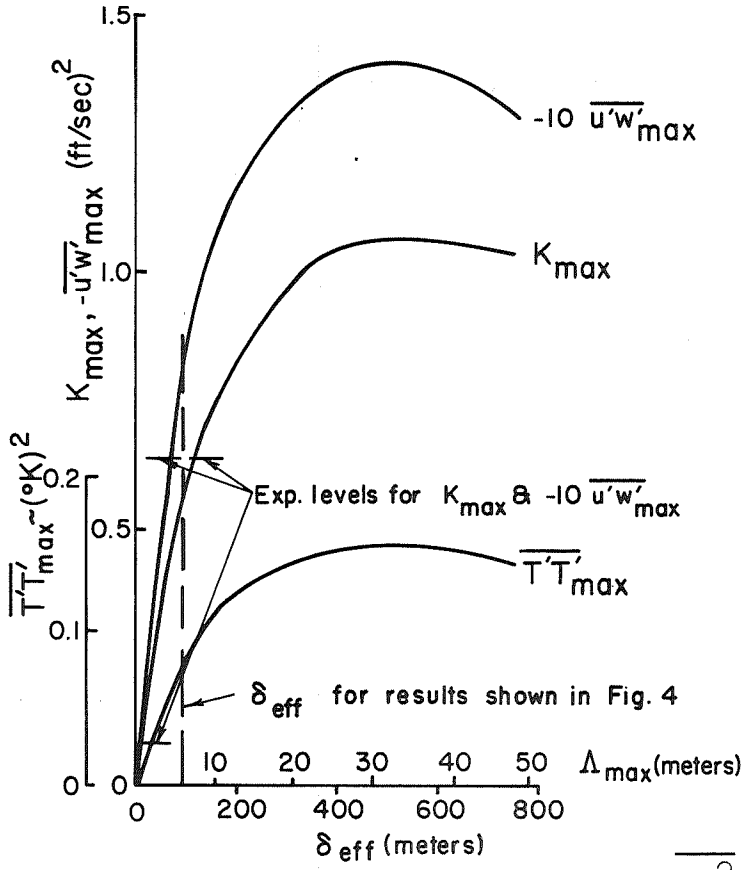

Figure 9.- Dependence of maximum values of $\overline{T'^2}$, $-\overline{u'w'}$, and K on the choice of δ_{eff} or Λ.

The second observation that may be made in regard to figure 9 is that we were fortunate in our choice of δ_{eff} in making the computations shown in figures 4, 5, and 6, for at this particular value of δ_{eff} fairly close agreement with experimental results is found. This is true, but even if one were to change the choice of δ_{eff} by a factor of two, one would still compute the proper order of magnitude of the values of the atmospheric turbulence parameters of interest.

The presentation of the effect of scale on the generation of atmospheric turbulence given in figure 9 shows the effect of scale only on the intensity of the turbulence. Increasing the scale of turbulence also rather markedly affects the distribution of turbulence intensity through increased diffusion, as mentioned above. This effect is demonstrated in figure 10 where we have plotted the distribution of the specific turbulent kinetic energy K as a function of altitude for three choices of δ_{eff} or Λ_{max}.

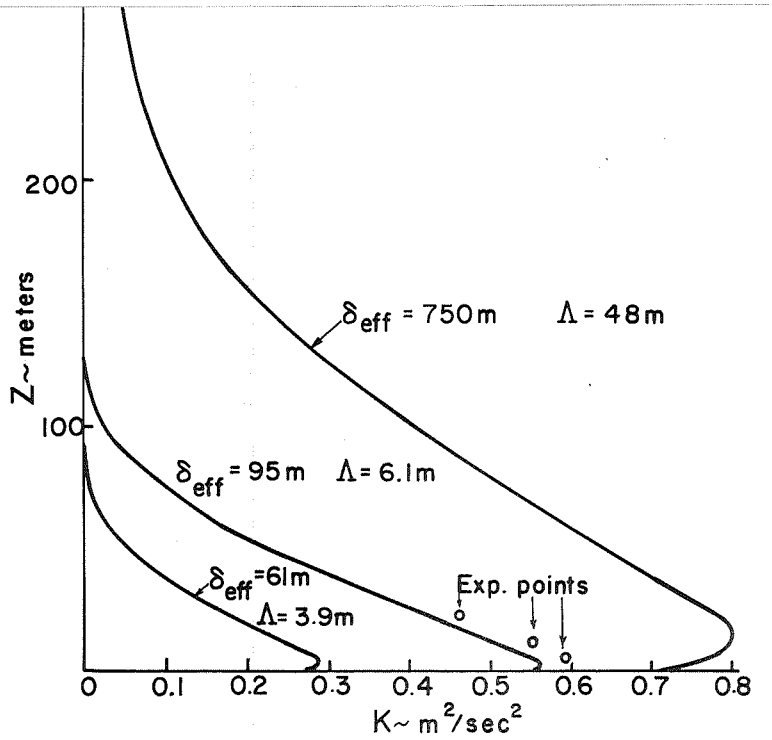

Figure 10.- Effect of the choice of δ_{eff} or Λ on the spread, as well as the intensity, of turbulence in the atmospheric boundary layer.

It is obvious from figure 10 that the scale Λ in our computations plays an important role in determining the intensity and distribution of turbulence produced by any mean shear profile in the atmosphere.

In view of the uncertainties present in defining the mean atmospheric boundary layers for which measurements have been made available to us by Wyngaard and Coté, we are encouraged by the results of a comparison of computed and measured results. In general, the correlations $\overline{u'u'}$, $\overline{v'v'}$, $\overline{w'w'}$, and $\overline{T'^2}$ which are computed agree with the experimental results within a factor of about two. Somewhat better agreement between theory and experiment is found for the transport correlations $\overline{u'w'}$, $\overline{u'T'}$, and $\overline{w'T'}$. It is felt that this agreement is sufficiently good to warrant further study and development of the method.

ATMOSPHERIC DISPERSION MODELING

The basic differential equation for the rate of change of the average concentration of a material p emanating from a source located at (x,y,z) and for straight-line atmospheric motions is

$$\rho_o \bar{u} \frac{\partial \bar{C}_p}{\partial x} = \dot{m}_p(x,y,z) + \frac{\partial}{\partial y}\left(\mu_o \frac{\partial \bar{C}_p}{\partial y} - \rho_o \overline{C_p'v'}\right) + \frac{\partial}{\partial z}\left(\mu_o \frac{\partial \bar{C}_p}{\partial z} - \rho_o \overline{C_p'w'}\right) \tag{15}$$

Equation (15) notes directly that the local change in concentration is equal to any local source rate of production of p less the divergence of the molecular and turbulent fluxes of p at (x,y,z). In order to convert (15) into a predictive model which can then be integrated over distance steps dx (or, equivalently, over time steps $\bar{u}\,dt$), it is necessary to develop predictive equations for $\overline{C_p'v'}$ and $\overline{C_p'w'}$. Since C_p is a scalar, the invariant technique for developing these predictive equations is completely analogous to the method used to predict the turbulent heat flux $\overline{w'T'}$ in developing the turbulence equations (ref. 5). In this derivation, the only new term which is added is $\overline{C_p'T'}$ and the dispersion equations are closed by modeling $\overline{C_p'v'}$, $\overline{C_p'w'}$, and $\overline{C_p'T'}$. The resulting equations for these terms are

$$\begin{aligned}
\rho_o \bar{u} \frac{\partial \overline{C_p'v'}}{\partial x} = {} & -\rho_o \overline{v'v'} \frac{\partial \bar{C}_p}{\partial y} + 3\frac{\partial}{\partial y}\left(\rho_o \Lambda \sqrt{K} \frac{\partial \overline{C_p'v'}}{\partial y}\right) \\
& + \frac{\partial}{\partial z}\left(\rho_o \Lambda \sqrt{K} \frac{\partial \overline{C_p'v'}}{\partial z}\right) + \frac{\partial}{\partial y}\left(\rho_o \Lambda \sqrt{K} \frac{\partial \overline{C_p'w'}}{\partial z}\right) \\
& + \frac{\partial}{\partial z}\left(\rho_o \Lambda \sqrt{K} \frac{\partial \overline{C_p'w'}}{\partial y}\right) - \frac{\rho_o \sqrt{K}}{\Lambda} \overline{C_p'v'} \\
& + \mu_o \left(\frac{\partial^2 \overline{C_p'v'}}{\partial y^2} + \frac{\partial^2 \overline{C_p'v'}}{\partial z^2} - \frac{2\overline{C_p'v'}}{\lambda^2}\right)
\end{aligned} \tag{16}$$

$$\rho_o \bar{u} \frac{\partial \overline{C_p' w'}}{\partial x} = -\rho_o \overline{w'w'} \frac{\partial \bar{C}_p}{\partial z} + \frac{\partial}{\partial y}\left(\rho_o \Lambda \sqrt{K} \frac{\partial \overline{C_p' w'}}{\partial y}\right)$$
$$+ 3 \frac{\partial}{\partial z}\left(\rho_o \Lambda \sqrt{K} \frac{\partial \overline{C_p' w'}}{\partial z}\right) + \frac{\partial}{\partial y}\left(\rho_o \Lambda \sqrt{K} \frac{\partial \overline{C_p' v'}}{\partial z}\right)$$
$$+ \frac{\partial}{\partial z}\left(\rho_o \Lambda \sqrt{K} \frac{\partial \overline{C_p' v'}}{\partial y}\right) - \frac{\rho_o \sqrt{K}}{\Lambda} \overline{C_p' w'}$$
$$+ \mu_o \left(\frac{\partial^2 \overline{C_p' w'}}{\partial y^2} + \frac{\partial^2 \overline{C_p' w'}}{\partial z^2} - \frac{2\overline{C_p' w'}}{\lambda^2}\right)$$
$$- (\mu_o + \mu_2)\left[\frac{1}{\rho_o}\frac{\partial^2 \rho_o}{\partial z^2} - \frac{2}{\rho_o^2}\left(\frac{\partial \rho_o}{\partial z}\right)^2\right] \overline{C_p' w'} + \frac{\rho_o g}{\bar{T}_o} \overline{C_p' T'} \qquad (17)$$

$$\rho_o \bar{u} \frac{\partial \overline{C_p' T'}}{\partial x} = -\rho_o \overline{w'T'} \frac{\partial \bar{C}_p}{\partial z} - \rho_o \overline{C_p' w'} \frac{\partial \bar{T}}{\partial z} + \frac{\partial}{\partial y}\left(\rho_o \Lambda \sqrt{K} \frac{\partial \overline{C_p' T'}}{\partial y}\right)$$
$$+ \frac{\partial}{\partial z}\left(\rho_o \Lambda \sqrt{K} \frac{\partial \overline{C_p' T'}}{\partial z}\right) + \mu_o\left(\frac{\partial^2 \overline{C_p' T'}}{\partial y^2} + \frac{\partial^2 \overline{C_p' T'}}{\partial z^2} - \frac{2\overline{C_p' T'}}{\lambda^2}\right) \qquad (18)$$

We may note immediately that for line sources oriented normal to the $\bar{u}$-direction, there is no net horizontal crosswind flux of material, and these equations reduce to a relatively simple, two-dimensional parabolic form. The full set, appropriate to point sources, is three-dimensional, however, and therefore requires a much larger computer capacity for numerical solution. The full set has been programmed for the Univac 1108; in addition, the reduced (line source) set has been programmed for the IBM 1130. This latter feature has permitted inexpensive parameter searches and initial exercising of the model for validation.

Basic Tests of the Diffusion Model

With the early approximate verification of turbulent correllations predicted by invariant modeling, attention has been directed to programming and exercising the diffusion models. In order to maximize the ability to vary the scale length parameters inherent in this modeling technique, the two-dimensional model was programmed and run extensively. This model, in its present configuration, is appropriate to simulation of the vertical diffusion of materials emitted from a continuous, infinitely long line source oriented perpendicular to the mean wind. It is referred to here as the LPD model (line pollution diffusion).

As an initial test, turbulence fields were selected from the AFCRL data and the diffusion model was run using the same values of scale lengths Λ and λ as were used in the turbulence simulation run. Initially the line source was simulated by a half-gaussian distribution with a standard deviation of 7 m and a maximum concentration located at 1.5 m above ground level (concentration values below 1.5 m were calculated by the model with a no-vertical-flux boundary condition at $z = 0$). The results of the calculation for the unstable atmosphere are shown in figure 11 where vertical profiles of concentration at distances of 180, 1500, and 4800 m from the source are portrayed. The general behavior of the model's concentration predictions were quite realistic, showing the expected spreading of the cloud upward and a diminution of the maximum concentration to less than one-tenth its initial value in less than 4800 m of travel. (Recall these calculations are for vertical diffusion only.) The only questionable feature is the displacement of the maximum concentration upward during this period of travel. Such displacements have been observed experimentally and are generally explained by an assumption of loss of material at the ground, a physical process which has not been incorporated in the LPD model.

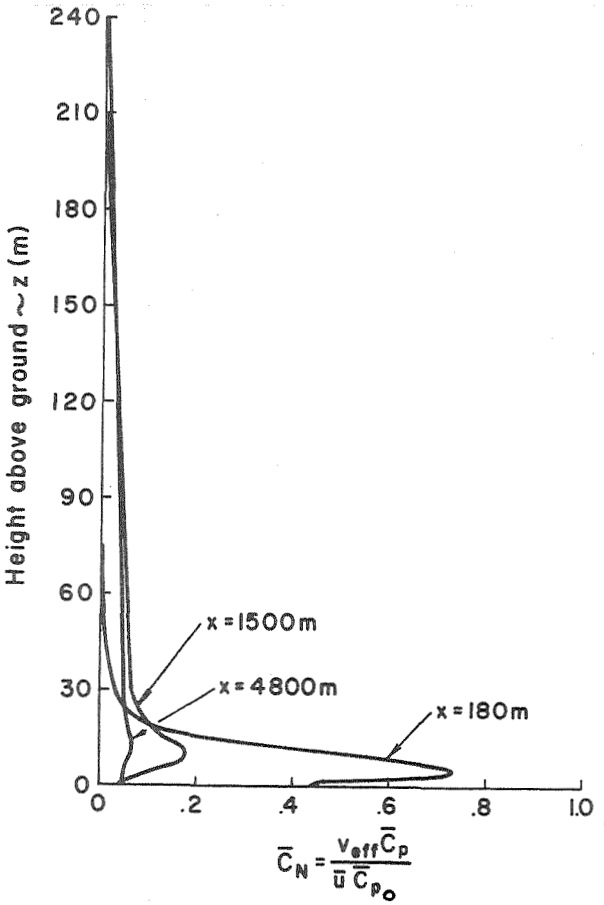

Figure 11.- Vertical profiles of concentration $\bar{C}_N$ for a cross-wind line source at 1.5 m above ground level.

Examination of the vertical profiles of turbulent flux $\overline{C_p'w'}$ generated by the model suggest that a more general parameter search for both Λ_{max} and for the coefficients which relate Λ_{max} to the dissipation scale length λ is required, particularly in the height zone near a solid boundary. This search has been initiated, but without conclusive results to date. In the meantime, the general behavior of the model is correct and the direction of improvement and refinement is known.

Initial programming of the three-dimensional diffusion model was completed during the course of this work, but no extensive use of the model has been undertaken. One run, using the same meteorological condition as for the LPD tests, has been estimated and is used in the next section to examine pollution patterns arising from idle, taxi, and takeoff modes of aircraft operations. A more extensive presentation of the results of the two-dimensional diffusion calculations is included as Appendix A.

Preliminary Dispersion and Concentration Calculations for Various Aircraft Operation Modes

Although major airports present a variety of sources of air pollution (e.g., fixed power plants, fuel dump spills and evaporation, ground vehicle operation, etc.), one of the sources of primary interest is aircraft engine exhausts. Varying amounts of various pollutants - such as unburned hydrocarbons, oxides of nitrogen, oxides of sulphur, and particulates - are emitted during operation of aircraft engines, the amounts ranging from maximum emission rates during full power takeoff runs to lesser amounts in idle and taxi operations. The pollutants and their emission rates also vary with engine type, size, and number. For our present purposes, however, primary interest focuses on the position and mode of motion of the aircraft. This is so simply because these motions determine the volume of air into which engine exhausts are discharged and, therefore, the effective initial source strength. If Q is the exhaust discharge rate (g/sec) of a pollutant, the effective source strength is Q/v_{eff} where v_{eff} is the speed of the aircraft relative to the air.

Engine exhausts are also considerably warmer than the ambient air and are usually discharged with a considerable velocity. Both of these features lead to an accelerated initial mixing of the exhaust products with the ambient air and consequent initial dilutions greater than those attributable to natural atmospheric turbulent mixing. Also, turbulence generated by the flow of air over the aircraft enhances this initial mixing rate. However, during takeoff and landing operations, a more prominent feature of aircraft-induced atmospheric motions is the wing tip vortices which entrap exhaust pollutants and generally tend to transport them downward against the buoyancy-induced upward motions of hot

gases. These features peculiar to aircraft operation have not yet been included in the present analyses, an omission which will tend to qualify any absolute values of pollutant concentrations. The preliminary calculations presented here are, therefore, more instructive as to the relative effects of atmospheric dispersion and aircraft operation modes as simulated by invariant modeling.

For this purpose, five modes of operation of a single aircraft have been chosen for preliminary simulation of pollutant concentration patterns due to engine exhausts:

1. A parked, idling aircraft away from terminals and hangers;
2. A constant speed, crosswind taxi operation;
3. A constant speed, upwind taxi operation;
4. A maximum power, upwind takeoff operation;
5. A constant speed, crosswind fly-by at 60 m above ground level.

For each of these simulations, calculated concentrations have been normalized to a unit exhaust emission rate and unit relative velocity between the aircraft and the atmosphere, i.e., where $\overline{C}_N$ is the normalized mass fraction of the pollutant and $\overline{C}_{po}$ is the initial value of $\overline{C}_p$.

$$\overline{C}_N = \frac{\overline{C}_p v_{eff}}{\bar{u}\overline{C}_{po}}$$

Since near-ground-level concentrations of pollutants are particularly important in adjusting operations to meet air quality standards, this feature of these preliminary calculations is stressed here. More detailed profiles of concentrations and the turbulent fluxes which produce diffusion are included in Appendix A.

A single meteorological case has been chosen for all of these calculations in order that attention may focus on comparisons of ground-level pollutant concentrations produced by different modes of aircraft operations. More detailed analyses of the effects of atmospheric stability and wind shear are proposed for future exercising of the model now that its basic utility and operability have been demonstrated.

Crosswind and Parked Aircraft Operations

The two-dimensional diffusion model may be used to simulate the pollution concentration patterns produced by aircraft that are moving along a path normal to the mean wind, either on the ground or in the air. Since primary interest focuses on pollution concen-

tration near ground level (in the breathing zone), we have emphasized that parameter. (The model, of course, predicts concentrations at all heights.)

Normalized ground-level concentrations for the cases of an aircraft taxiing crosswind and of an aircraft flying at 60 m above the surface are shown in figure 12. Both cases are for an unstable atmosphere. The general decrease of concentration downwind of the taxi path followed by the aircraft is quite reasonable but requires experimental verification. The ground-level concentrations caused by the fly-by also properly portray the mixing of the pollutant to ground level, but appear to maintain a near-constant value over too great a distance.

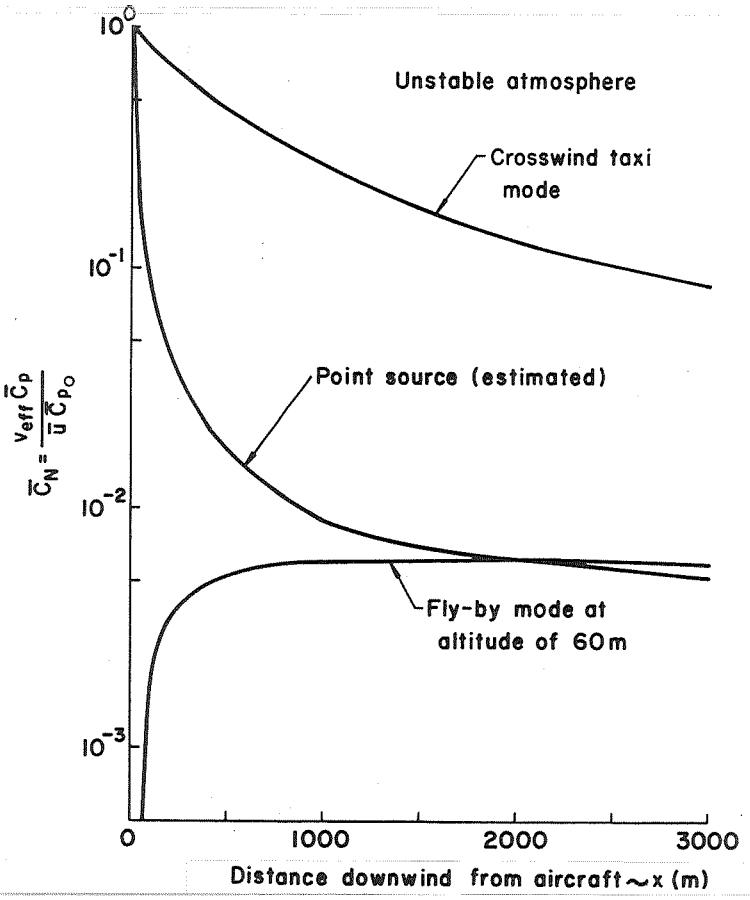

Figure 12.- Simulated values of maximum ground level concentration of engine exhausts when the aircraft is 1) parked (point source), 2) taxiing crosswind, and 3) flying crosswind at 60 m .

Of greater interest from an operational point of view is the effect of the altitude of the source on ground-level concentrations. In this case, the relative maximum concentration produced by the two source positions is 167, a result which suggests that, with the additional factor of airspeed considered, aircraft-produced ground-level pollution near airports is primarily caused by ground operation of those aircraft, and their contribution while airborne is relatively small.

The maximum ground level concentrations of engine exhausts produced by an aircraft parked on the ground with engines running are also shown in figure 12. This operational mode is simulated by the three-dimensional model, and the enhanced dilution rate occasioned by the addition of lateral as well as vertical diffusion is quite evident.* As a result of lateral diffusion, concentrations of exhausts from this essentially stationary source are considerably less than for the taxiing case just shown. This result must be interpreted operationally, however, since the total exposure to pollutants depends upon the duration of the exposure to these concentrations. If the effect of a pollutant on the receptor depends on the total dosage, these concentrations must be multiplied by the time of exposure. This time will be brief (seconds) for the taxi mode but will be approximately equal to the time the aircraft is parked for that mode.

Again, from an operational point of view, we may note that a long line of parked, idling aircraft aligned crosswind will approximate to a continuous line source. In this situation, lateral diffusion will be minimized, concentrations will be high, and duration of exposure will be long. An operational choice for this circumstance could be the spacing of the aircraft so that at least the initial lateral diffusion can operate. The effectiveness of such a technique can be readily evaluated by the type of model being developed here.

Upwind Taxi and Takeoff Operations

The profile of maximum concentration produced by a fixed point source (the parked, idling aircraft) provides the basis for simulating dosage patterns for aircraft in motion along the direction of the wind. In these operations it is desirable to consider dosage rather than average concentration since the time of exposure depends upon the position of the receptor relative to the path of the aircraft. For example, a receptor at the downwind end of a runway or taxi strip will be exposed to all of the exhaust emitted upwind of him during a taxi or takeoff operation. A second receptor

---

*The lateral diffusion for calculation of $\overline{C}_{p\ max}$ from a point source has been estimated due to operational difficulties with the three-dimensional model.

located upwind of the first will be exposed to only those emissions generated after the aircraft has passed his position.

The maximum dosage is defined as the integral of the concentration over time

$$D_{max} = \int \overline{C}_{p_{max}} \, dt$$

where $\overline{C}_{p_{max}}$ is now the time history of maximum concentration produced at a fixed point due to all sources upwind of that position. In the present calculations, $\overline{C}_{p_{max}}$ is normalized to an initial value (at the moving source) of unity when the source strength (mass rate of emission) and the effective velocity of the source are also unity.

The simulation of dosages is accomplished by convoluting the maximum concentration profile and the amount emitted per unit distance of travel. Since the amount emitted per unit distance of travel is inversely proportional to the effective velocity of the aircraft, the convolution is

$$D_{max}(x) = \int_0^\infty \frac{\overline{C}_p(x|\xi)}{V_{eff}(\xi)} \, d\xi$$

where x is the position of the fixed receptor and ξ is the position of the moving source. Since the emitted material is assumed to move with the mean wind speed $\bar{u}$, the time of exposure over which the dosage D_{max} is delivered τ is given by

$$\tau(x) = \frac{1}{\bar{u}} \int_{x=\xi}^{\xi_{max}} d\xi \qquad \xi \geq 0$$

and an average concentration may be defined for each x by

$$\overline{\overline{C}}_{p_{max}}(x) = \frac{D_{max}(x)}{\tau(x)}$$

For the purposes of the present illustrations, we have assumed 1) an upwind taxi run at a constant speed equal to the mean wind speed ($V_{eff} = 2\bar{u}$), and 2) an upwind take-off run for

which the takeoff speed profile is shown in figure 13.* The resulting normalized dosages from the upwind end of the runway (point of takeoff or cessation of taxi run) to one runway length downwind of the runway are shown in figure 14. These curves point up quite vividly the build-up of the maximum dosages (all of the material emitted during either operation must pass through a plane transverse to the origin or the position at which the operation begins). Downwind of the origin, atmospheric dilution reduces the maximum concentrations or dosages in the expected manner.

The differences in dosage patterns along the runway are all due to the difference in the speed profiles. In particular, the acceleration for the takeoff run reduces the emission per unit distance of travel markedly over the constant-speed taxi operation. (Total emission rates may, of course, vary drastically between these operations.) From an operational point of view, the maximum at the downwind end of the runway and the dosages or concentrations downwind of this position are of primary concern. For example, with a wind speed of 5 m/sec and a mass fraction of exhaust pollutant of 100 parts per million ($\overline{C}_{po} = 10^{-4}$), the maximum average concentration at $x = 0$ is about $0.5 \times 10^{-4} \times 3 \times 10^{-3} = 1.5 \times 10^{-7}$, or the order of 150 pphm.

However, the primary intent here is to illustrate the capability of simulation modeling to portray air pollution patterns associated with various airport operations. More rigorous verification of these patterns and the opportunity to match the "free" parameters of invariant modeling are, of course, required. However, this initial effort shows great promise for realistic simulations of complex situations.

*Both of these calculations are for a unit emission rate, $\dot{m}_p$.

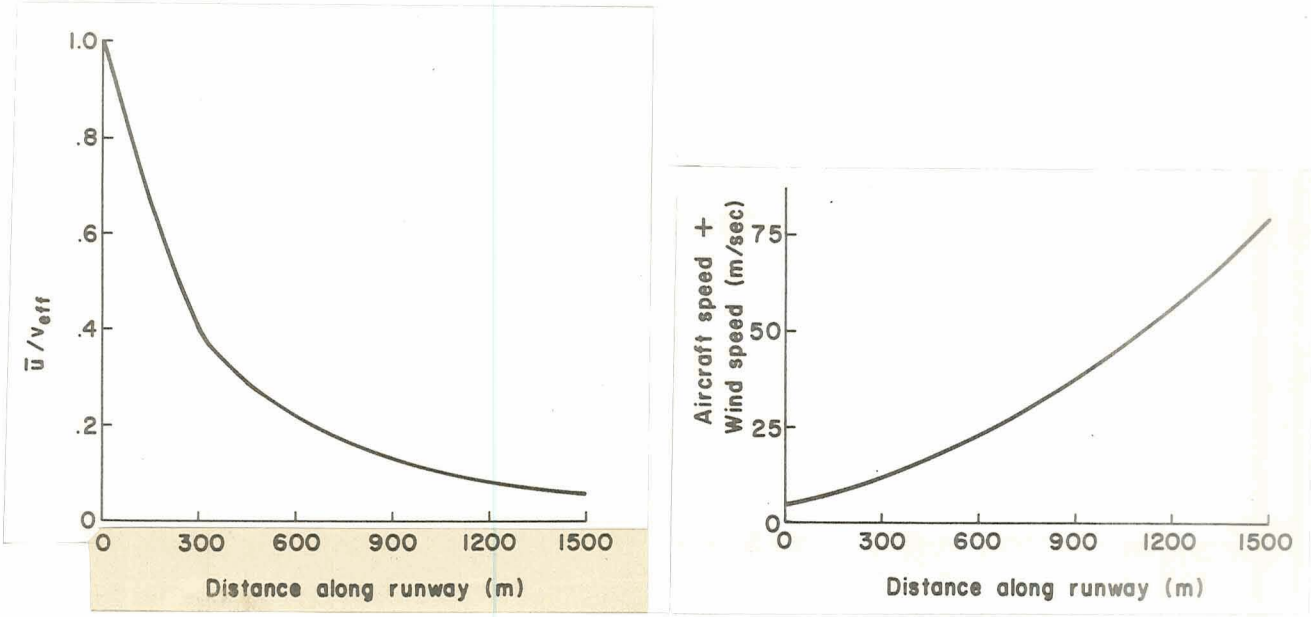

Figure 13.- Assumed aircraft speed profile for take-off run and resultant ratio of wind speed $\bar{u}$ and airspeed v_{eff} used in computing dosages resulting from exhaust emissions during take-off.

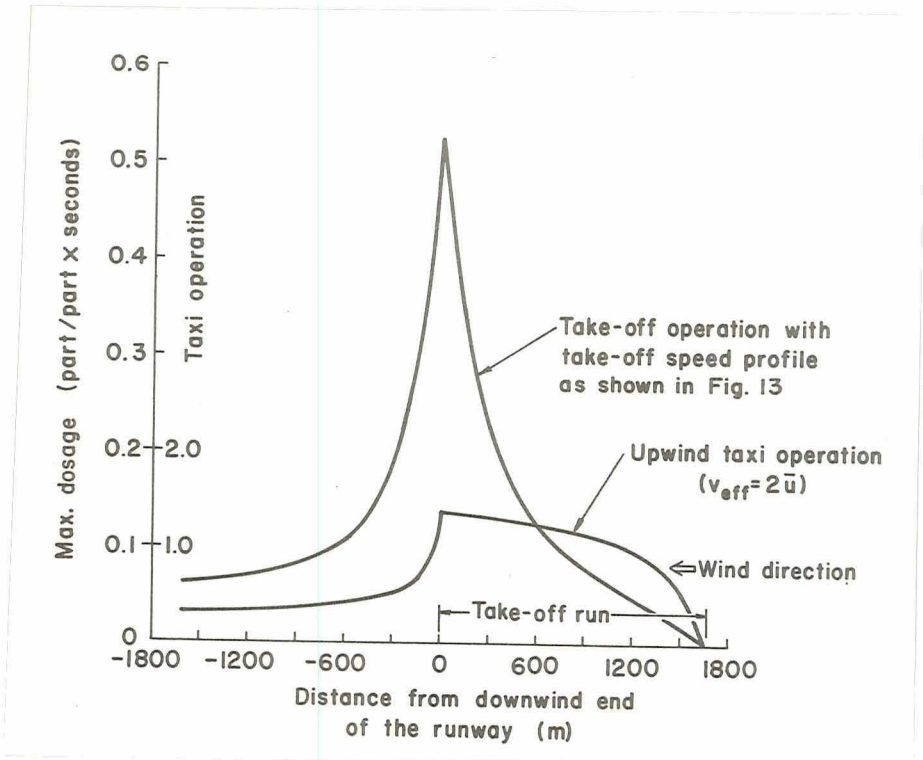

Figure 14.- Ground level dosage patterns associated with upwind taxi and take-off operations.

CONCLUSIONS

The work reported here must be viewed as an early and relatively primitive test of the ability of the invariant modeling method to simulate the turbulent structure and diffusive capabilities of a turbulent atmospheric boundary layer. Despite the early stage of this work, the results show a high degree of promise and it appears that useful simulation of the atmosphere with only a minimum of input information and arbitrarily specified coefficients can be developed. The ability of coefficients established for a low speed, constant-temperature flat plate boundary layer to produce correct order of magnitude predictions for the planetary boundary layer when the stability is not neutral suggests the real power of the invariant modeling technique. The ability to simulate fluxes of heat, momentum, and matter without detailed input information on exchange rate coefficients also emphasizes the degree to which invariant modeling has captured the essential physics of turbulent boundary layer processes.

The application of these techniques to airport-oriented air pollution problems associated with aircraft operations has been illustrated. Refinements of the model to include the effect of heated exhausts and aircraft-induced turbulence are possible and will be important in those cases where short-lived transient air pollution concentration patterns dictate permissible modes of operation at airports.

With this essential demonstration of the basic correctness and feasibility of invariant modeling, work can proceed confidently towards the further refinement of these early results and the testing of turbulence and diffusion modeling for more complicated real-world situations. Completion of the three-dimensional simulation model is more a matter of devoting the required resources of manpower and computer time than of technical problems. The program is large and complex and has not yielded easily to debugging and check-out.

A major parameter search, designed to match model predictions of motions and fluxes in free jets to observational evidence has been completed and can now be extended to boundary layer modeling. These steps should provide improved simulation of the second-order correlation profiles in unstable atmospheres. Definite improvements in the prediction of the distribution of matter from arbitrary sources are also expected. With the full development of these refinements, the diffusive properties of arbitrarily stratified atmospheres can be examined.

APPENDIX A

SUMMARIES OF CALCULATIONS OF TURBULENCE CORRELATIONS AND ATMOSPHERIC DIFFUSION

In order to provide the reader interested in the detailed information generated by the invariant turbulence and diffusion modeling, we have selected one run for which machine graphics of the model outputs have been assembled. This case is for stably stratified atmosphere and the diffusion of material emitted from an infinitely long, near ground-level area source of 1500 m width and oriented across the mean wind direction. This case has no exact analogy in airport operations, except perhaps to treat the entire airport as an area source. The line source diffusion model is appropriate to this case up to distances of about ten times the actual crosswind length of the area source.

The mean wind and temperature profiles used in this calculation are shown in figures 1A and 2A, and the vertical fluxes calculated by the invariant turbulence model, $\overline{u'w'}$, $\overline{u'T'}$, $\overline{w'T'}$, and $\overline{T'T'}$ are also shown. The turbulent energies $\overline{u'u'}$, $\overline{v'v'}$, and $\overline{w'w'}$ are shown in figure 3A. These are the primary turbulent correlations which enter into the diffusion model and, as noted in the text of this report, these values are exceptionally well matched with experimental measurements. Figure 4A shows the time history of the model generation of the turbulent energies. As can be seen there, equilibrium values were reached very early in the calculation.

Turning to the diffusion calculations, a line source was simulated with an initial vertical distribution given by

$$\dot{m}_p = 1 - \left(\frac{z - z_o}{D} \right)^2 \cdot A$$

where z_o and D are lengths chosen to place z_o, the height of the maximum $\overline{C}_{po}$, at 15 m above the surface and C_{po} at $z = 0$ and $z = 30$ m.

The cumulative concentrations and the vertical profiles of $\overline{C_p'w'}$ and $\overline{C_p'T'}$ at the downwind edge of this area source are portrayed in figure 5A. Figure 6A shows these same profiles at a distance of about 3500 m downwind from the upwind edge of the source. At this distance, vertical diffusion has produced a half-gaussian distribution of $\overline{C}_p(z)$ with the maximum near the ground and the vertical turbulent flux $\overline{C_p'w'}$ is positive.

Figure 7A provides a plot of concentration $\overline{C}_p$, $\overline{C_p'w'}$, and $\overline{C_p'T'}$ at $z \simeq 2.5$ m out to a distance of 15,000 m. $\overline{C}_p$ increases over the source area, then decreases exponentially with distance as vertical diffusion operates on the cloud. In figure 8A, the maxima of $\overline{C}_p$, $\overline{C_p'w'}$, and $\overline{C_p'T'}$ are plotted versus distance out to 15,000 m.

These examples could be elaborated indefinitely, of course, but they do provide illustrations of the detailed aspects of turbulence, turbulent fluxes, and resulting concentration distributions as simulated by invariant modeling. Relatively simple initial distributions of these terms have been chosen for these early calculations. In principle, arbitrary and more complex situations can be handled by the modeling technique. This is not true for more conventional diffusion models. However, exercising of the invariant models can provide very valuable insight as to physical processes and the engineering approximations required for more heuristic modeling systems.

REFERENCES

1. Environmental Quality, the First Annual Report of the Council on Environmental Quality, Transmitted to the Congress, August 1970 (available from U.S. Government Printing Office).

2. Letter to J.E. Duberg, NASA, from C.duP.Donaldson, A.R.A.P., dated March 23, 1970 (incorporated by reference in Contract NAS1-10192).

3. Letter proposal to G.L.Smith, NASA, from C.duP.Donaldson, A.R.A.P., dated March 19, 1971.

4. Donaldson, Coleman duP.; and Rosenbaum, Harold: Calculation of Turbulent Shear Flows Through Closure of the Reynolds Equations by Invariant Modeling. A.R.A.P. Report No. 127, December 1968.

5. Donaldson, Coleman duP.; Sullivan, Roger D.; and Rosenbaum, Harold: Theoretical Study of the Generation of Atmospheric Clear Air Turbulence. AIAA Paper No. 70-55, presented at the AIAA 8th Aerospace Sciences Meeting, New York, January 19-21, 1970 (accepted for publication in AIAA Journal).

6. Donaldson, Coleman duP.: Calculation of Turbulent Shear Flows for Atmospheric and Vortex Motions. AIAA Paper No. 71-217, presented at the AIAA 9th Aerospace Sciences Meeting, New York, January 25-27, 1971, as the Dryden Research Lecture (accepted for publication in AIAA Journal).

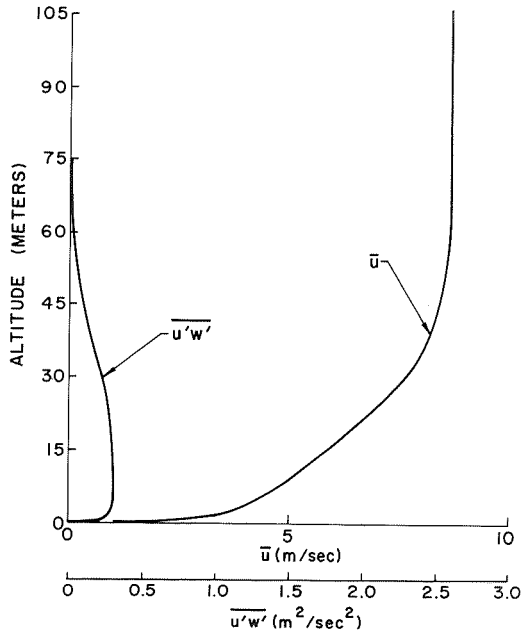

Figure 1A. Vertical profile of turbulent shear stress $\overline{u'w'}$ generated by the model for the mean wind speed and temperature profiles shown here and in figure 2A.

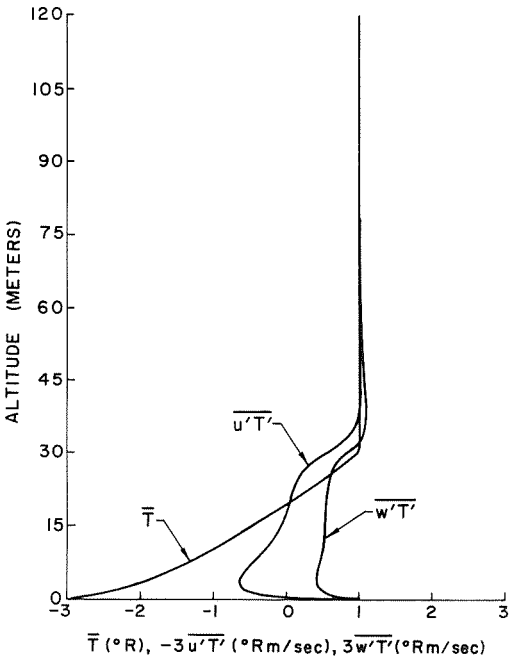

Figure 2A. Vertical profiles of the turbulent flux of heat in the longitudinal ($\overline{u'T'}$) and vertical ($\overline{w'T'}$) directions predicted for the mean wind and temperature profiles shown here and in figure 1A.

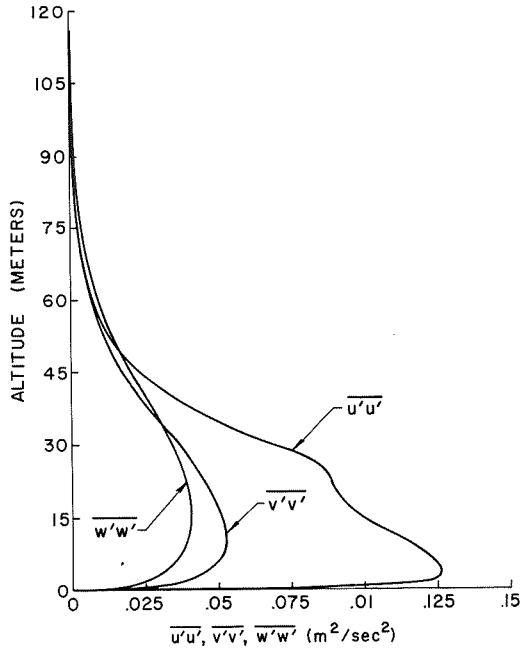

Figure 3A. Vertical profiles of turbulent energies in the longitudinal ($\overline{u'u'}$), lateral ($\overline{v'v'}$), and vertical ($\overline{w'w'}$) directions predicted for the mean wind and temperature profiles shown in figures 1A and 2A.

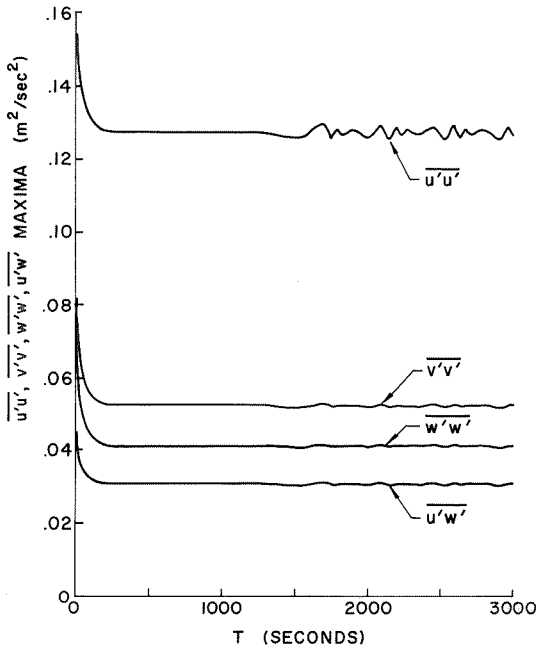

Figure 4A. Time steps required for the model to come to equilibrium after introduction of a small component of turbulence.

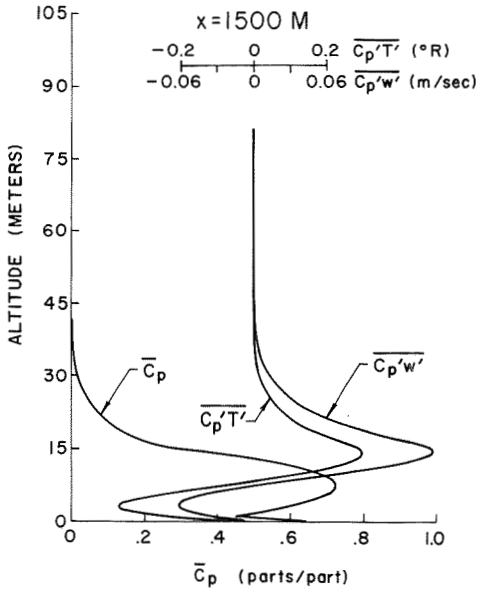

Figure 5A. Vertical profiles of pollutant concentrations, $\overline{C}_p$, and of the correlations, $\overline{C_p'T'}$ and $\overline{C_p'w'}$, at a travel distance of 1500 m. The pollutant was introduced as an infinite crosswind area between $X = 0_x$ and $X = 1.5$ km.

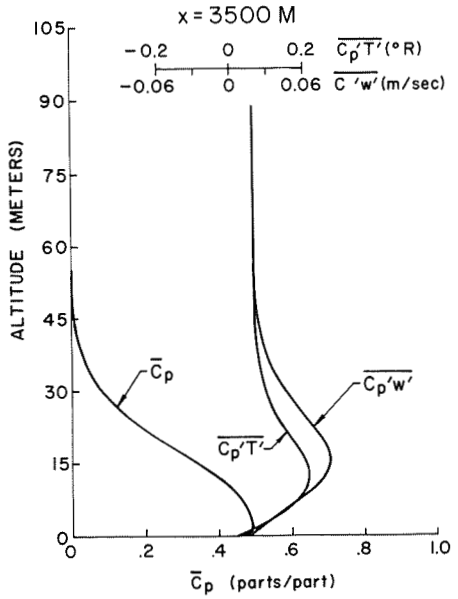

Figure 6A. Same as 5A except that $X = 3500$ m.

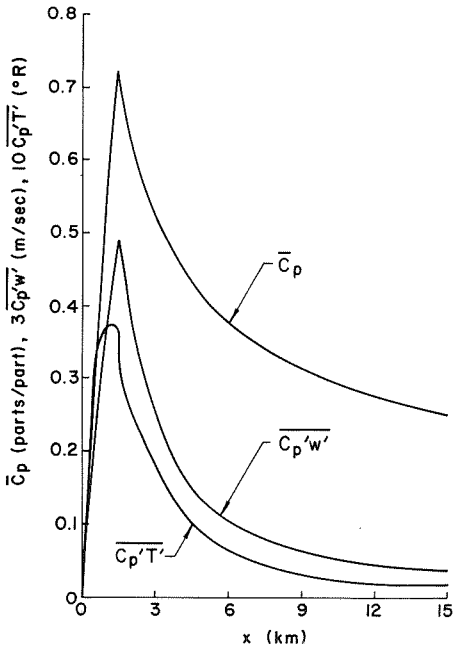

Figure 7A. Values of $\bar{C}_p$, $\overline{C_p'w'}$, and $\overline{C_p'T'}$ as a function of distance from the source area and at a height of 2.5 m above the ground.

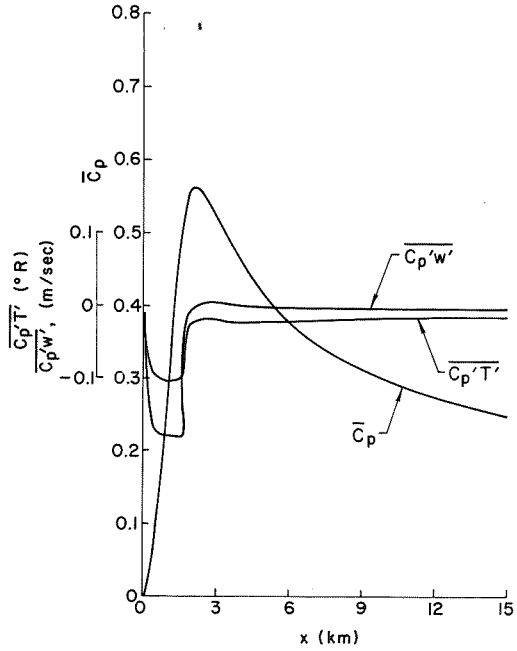

Figure 8A. Maximum values of $\bar{C}_p$, $\overline{C_p'w'}$, and $\overline{C_p'T'}$ as a function of distance from the source area.